Depinning Dynamics of Crack Fronts

Julien Chopin*
Gulliver UMR 7083, CNRS-ESPCI ParisTech, PSL Research University, Paris, France
Institut Jean le Rond d'Alembert UMR 7190, Sorbonne Universités, CNRS-UPMC, Paris, France
and Instituto de Física, Universidade Federal da Bahia, Campus Universitário de Ondina, rua Barão de Jeremoabo, BA 40210-340, Brazil

Aditya Bhaskar, Atharv Jog, and Laurent Ponson†
Institut Jean le Rond d'Alembert UMR 7190, Sorbonne Universités, CNRS-UPMC, Paris, France

(Received 6 September 2018; published 7 December 2018)

We investigate experimentally and theoretically the dynamics of a crack front during the microinstabilities taking place in heterogeneous materials between two successive equilibrium positions. We focus specifically on the spatiotemporal evolution of the front, as it relaxes to a straight configuration, after depinning from a single obstacle of controlled strength and size. We show that this depinning dynamics is not controlled by inertia, but instead by the rate dependency of the dissipative mechanisms taking place within the fracture process zone. This implies that the crack speed fluctuations around its average value v_m can be predicted from an overdamped equation of motion $(v - v_m)/v_0 = [G - G_c(v_m)]/G_c(v_m)$ involving the characteristic material speed $v_0 = G_c(v_m)/G_c'(v_m)$ that emerges from the variation of fracture energy with crack speed. Our findings pave the way to a quantitative description of the critical depinning dynamics of cracks in disordered solids and open up new perspectives for the prediction of the effective failure properties of heterogeneous materials.

DOI: 10.1103/PhysRevLett.121.235501

Woods, nacre, bones, or rationally designed artificial materials, are all heterogeneous solids, with mechanical properties far exceeding those of their constitutive components. Understanding the role of microscale heterogeneities on the macroscale fracture behavior of solids still remains a query. This becomes especially relevant now, as rapid developments in microfabrication techniques allow the tailoring of microstructures at ever smaller scales, yielding new types of composites, known as metamaterials, with unprecedented mechanical properties [1–6]. Recently, significant progress was made for weakly heterogeneous brittle solids where models describing a crack front as a deformed interface pinned by tough obstacles have been successfully applied [7–11]. The homogenized fracture properties can be computed exactly within the so-called weak pinning limit [12], where the elastic energy release rate G balances the fracture energy G_c at any time and any position along the front. This approach holds for weak variations of toughness along the propagation direction. The crack evolution is then smooth and can be properly approximated by a continuous succession of equilibrium front configurations [13,14]. This approach was successfully used to design weakly heterogeneous systems with improved and new macroscopic failure properties [15–18].

However, most natural and engineered materials have a microstructure composed of discontinuous heterogeneities which cannot be described within the weak pinning regime. The strong pinning regime that predominates for large toughness gradients challenges standard homogenization approaches. Crack propagation is not quasistatic but proceeds by intermittent and local microinstabilities. Further, for a disordered distribution of obstacles, crack growth takes place close to the so-called depinning critical transition [19–21], so that the crack front dynamics is dominated by avalanches spanning over a large range of length and time scales [22–26]. The precise understanding of the front evolution during these rapid events is a prerequisite to predict and further, to control the fracture energy of heterogeneous solids. Beyond fracture, the behavior of driven disordered mechanical systems with long-range interactions is still an open question whose tremendous difficulty resides in the subtle interplay between fast, localized, depinning events and larger macroscopic avalanches forming a complex energetic landscape composed of many metastable states [27–29].

In this Letter, we address experimentally and theoretically the basic problem of the interaction of a crack front with a tough obstacle in the strong pinning regime. In our experiment, a planar crack is driven at a constant speed over a tough region of finite length along the propagation direction, triggering a depinning instability between two well-defined metastable states. The size and strength of the obstacles are fully controlled and adjusted using our patterning technique. The sample allows *in situ* visualization of

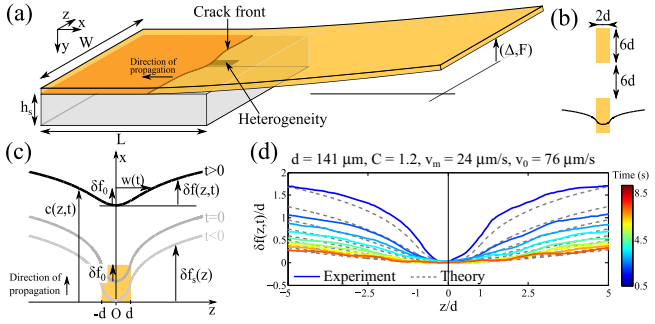

FIG. 1. (a) Schematics of the experimental setup showing an interfacial crack front pinned by a heterogeneity. (b) Rectangular obstacles of larger toughness. (c) $c(z,t)$ and $\delta f(z,t) = c(z,t) - c(0,t)$ are the crack front profile and deformation, respectively. $\delta f_s = \delta f(z, t < 0)$, $\delta f_0 = \delta f(d, 0)$ and $w(t)$ are the pinned (stationary) crack front deformation, the characteristic height, and half-width, respectively. (d) Sequence of crack front deformation after depinning and theoretical prediction.

the crack front dynamics which is resolved spatially and temporally.

After normalizing all the length scales by the obstacle width d, we show that the relaxation dynamics follows a universal law which only depends on v_0, the crack speed at depinning for an obstacle of unit strength. v_0 is also found to vary linearly with the crack speed v_m imposed prior depinning by the loading rate. Next, we develop a theoretical model based on linear elastic fracture mechanics to quantitatively capture the observed behavior. Here, inertial effects can be neglected as the crack speed remains several orders of magnitude lower than the wave speed. Instead, we take into account the *rate dependency* of the fracture energy to quantitatively capture the effect of crack speed on the dissipative mechanisms taking place within the process zone. Thus, unlike perfectly brittle solids, crack may propagate at finite speed in dissipative materials as the elastic energy release rate may be constantly balanced by a rate-dependent fracture energy. Linearizing the equation of motion around v_m, we obtain an analytical solution for the depinning of a crack from a single obstacle that is shown to capture quantitatively all our experimental observations. The implications of our results on the energy dissipated during fast fracture events and the fracture behavior of materials with randomly distributed obstacles are discussed in the final part of our Letter.

We start by describing our experimental setup. A 5 mm plate made of polymethylmethacrylate (PMMA, Young modulus $E_p = 1.8$ GPa) with a heterogeneous coating is detached from a thick elastomer block using the beam cantilever geometry shown in Fig. 1(a). A vertical upward pointlike force is exerted at the extremity of the PMMA plate by means of a string connected to a mechanical testing machine allowing us to impose the deflection speed. The elastomer is a cross-linked polydimethylsiloxane (PDMS Sylgard184, Dow Corning) with a much lower Young modulus $E_s = 1.5$ MPa than PMMA and a Poisson's ratio $\nu_s \simeq 0.5$. It is prepared by mixing an oligomer together with a silicon oil and degased for 2 h under mild vacuum. It is then cured in an oven at 75 °C for at least 2 h. The resulting cross-linked PDMS block of size $W \times L = 50 \times 80$ mm^2 with thickness $h_s = 20$ mm is then demoulded. The crack is driven at an average speed v_m in the range 5–100 μm/s that is set by the deflection rate imposed by the testing machine.

Taking inspiration from the experiments of Xia *et al.* [10,15], we control the local fracture properties of the interface by printing obstacles on a commercial transparency, taking advantage of the high toughness G_{c1} of the printed regions on PDMS compared to the neat one noted G_{c0}. Unlike G_{c1}, which does not show significant variations with the crack speed v_m, G_{c0} is found to increase as v_m^γ where $\gamma = 0.37 \pm 0.05$ [30]. The microscopical origin of the exponent is still highly debated [31,32]. As a consequence, the contrast $C = (G_{c1} - G_{c0})/G_{c0}$ can be varied by exploring different crack speeds. As shown in Fig. 1(b), rectangles of width $2d$ and length $6d$ are aligned along the propagation direction where d is varied between 0.1 and 0.5 mm. A spacing of $6d$ between two successive obstacles is chosen to allow a complete relaxation of the front before it reaches the next obstacle. The transparency is then bonded onto the PMMA plate by means of a double-sided adhesive tape, the heterogeneous side faced up. Finally, a thin liquid film of PDMS is laid on the substrate before bringing the coated PMMA plate in contact allowing an intimate bonding between materials after curing at 40 °C for 48 h.

The transparency of the materials used in our setup is exploited to visualize the front geometry and its evolution as it interacts with the obstacle. Images of 3900×2600 pixels are taken normal to the mean fracture plane by a CCD camera through a semitransparent mirror oriented at 45°. An LED panel is placed horizontally beneath the sample to increase the contrast between the bonded and unbonded regions of the interface. A homemade algorithm extracts then the crack position $c(z,t)$ for each image taken at time t where the depinning onset defines $t = 0$ [see Fig. 1(c)]. The front deformation is defined as $\delta f(z,t) = c(z,t) - c(0,t)$. An acquisition rate of 10 Hz allows resolving in detail the front evolution during the depinning regime.

In a typical experiment, the front propagates initially in a homogeneous interface as a straight line. For the range of velocity explored, no stick-slip instability occurs [33]. When crossing the obstacle, the profile gradually deforms until reaching a stationary shape composed of a pinned region of amplitude $\delta f_0(C,d)$ and logarithmic tails $\delta f_s(z) \simeq 2\delta f_0(C,d)\ln(|z|/d)$ for $|z| \gg d$. For weak obstacles, $\delta f_0(C,d)$ varies linearly with C but nonlinearities appear when C is finite, yielding $\delta f_0(C,d) = dC_{\mathrm{NL}}/\pi$, where $C_{\mathrm{NL}} = C(1 - C/2 + C^2/6)$ [8,8,9,11,34,35]. When reaching the end of the obstacle, the crack front is suddenly out of

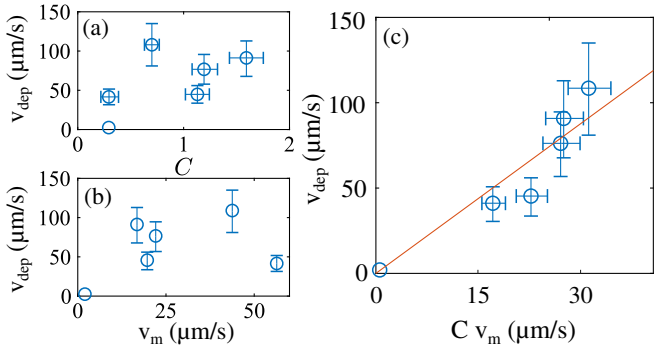

FIG. 2. Depinning velocity v_{dep} defined as the jump in crack speed as the front escapes from the obstacle varying (a) C and (b) v_m. (c) v_{dep} increases linearly with Cv_m.

equilibrium as the deformed profile is not stable in a homogeneous interface. We observe a fast motion of the pinned region and a slower motion of the remote part resulting in a relaxation towards a straight configuration [Fig. 1(d)]. This behavior is reminiscent of avalanches which are sudden fracture events observed between metastable configurations in fully disordered materials driven close to the so-called depinning transition [23,25,27]. We will see later that both phenomena are actually closely related.

We first focus on the initial dynamics of the instability measuring the depinning velocity v_{dep} defined as $v_{dep} = dc_{|z|<d}/dt|_{t=0^+} - v_m$ where $c_{|z|<d}$ is the front position averaged over $|z| < d$. While most experimental and numerical studies only report averaged quantities such as avalanches duration and size, here we have access to the entire dynamics. We found that v_{dep} is not uniquely determined by either v_m or C as indicated by the nonmonotonic behavior shown in Figs. 2(a) and 2(b). However, in Fig. 2(c), we show that v_{dep} is linearly depending on Cv_m as revealed by the good collapse of the data onto a line of slope $v_{dep}/(Cv_m) = v_0/v_m = 3.1$, where $v_0 = v_{dep}/C$ is the depinning velocity for an obstacle of unit strength.

Next, we address the relaxation dynamics at longer times beyond the onset of instability. We first measure the amplitude $\delta f(d,t)$ of the front deformation, and its evolution during depinning [see Fig. 1(c)]. As shown in the inset of Fig. 3(a), we observe that $\delta f(d,t)$ relaxes towards zero at a rate strongly depending on v_m and C. However, we found a good collapse of the relaxation profiles by normalizing $\delta f(d,t)$ and t by $C_{NL} \times d$ and d/v_m, respectively. These rescalings are found to be also relevant for the evolution of the half-width $w(t)$ of the perturbation, where $w(t)$ is defined from the relation $\delta f[w(t),t] = \delta f_s(d)$ [see Fig. 1(c)]. Here, $w(t)$ quantifies the lateral spreading of the perturbation through time. As shown in Fig. 3(b), we also find a good collapse of the data normalizing $w(t)$ by d. Further, after a short transient, the width is found to grow linearly with time, following $w(t) = 5.7v_m t$.

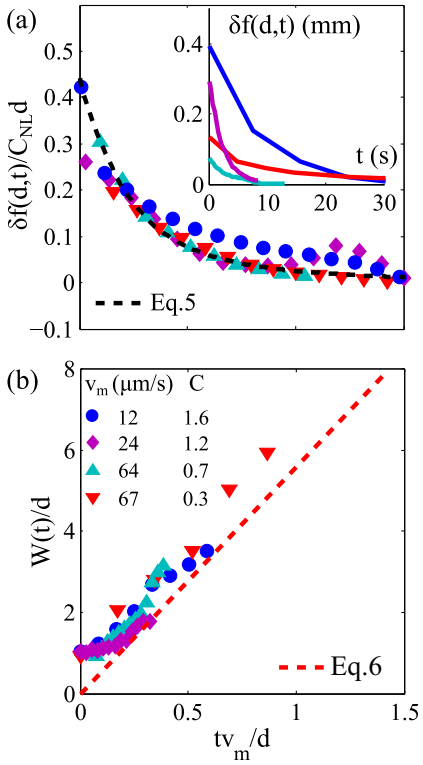

FIG. 3. (a) Relaxation of the normalized deformation amplitude with theoretical prediction (dashed line). Inset: data before normalization. (b) Spreading of the deformation width $w(t)$ and theoretical prediction (dashed line).

To explain quantitatively the observed dynamics, we develop a model within the framework of linear elastic fracture mechanics (LEFM) including a physically based dissipation mechanism to account for the viscoelastic dissipation in the process zone (PZ). Imposing that the energy release rate is balanced by the dissipated work within the PZ, the equation controlling crack evolution reads

$$G[c(z,t)] = G_c[c(z,t), v(z,t)]. \quad (1)$$

Here, G_c not only depends on the crack configuration $c(z,t)$ resulting from the interaction of the front with the obstacle, but also on the local speed $v(z,t) = \partial c(z,t)/\partial t$ owing to the rate dependency of the dissipation. A first-order perturbation of Eq. (1) around the mean front position $v_m t$ yields $\delta G[\delta c] = \{[\partial G_c(v_m)]/(\partial v)\}\delta v$, where $\delta c(z,t) = c(z,t) - v_m t$ and $\delta v(z,t) = v(z,t) - v_m$. The left-hand side term corresponds to a nonlocal elastic restoring force [36] while the right-hand side term represents a local friction term increasing linearly with v. Terms such as $[(\partial G_c)/(\partial c)]$ are not relevant since depinning occurs in a homogeneous region of the interface. The fracture toughness is taken in the form of $G_c = G_c^0(v/v_c)^\gamma$, where G_c^0, γ, and v_c are material parameters characterizing the dissipation mechanisms taking place in the process zone. Upon

linearization of G_c around the macroscopic driving velocity v_m in a slow propagation regime $v_m \ll v_c$, we obtain

$$\frac{1}{G_c^0}\frac{\delta G_c}{\delta v} \equiv \frac{1}{v_0} = \frac{\gamma}{v_m}. \tag{2}$$

Here we take $\gamma = 1/3$ in agreement with the value measured for the neat regions of the interface between the PDMS substrate and the cantilever [30]. Using the expression of δG derived for an interfacial crack between an incompressible substrate and a much stiffer material [37], we obtain the equation of motion

$$\frac{1}{v_0}\frac{\partial \delta c(z,t)}{\partial t} = \frac{1}{\pi} PV \int_{-\infty}^{+\infty} dz' \frac{\delta c(z',t) - \delta c(z,t)}{(z'-z)^2}. \tag{3}$$

At the linear order, Eq. (3) is formally equivalent to the equation of motion of a contact line of Newtonian fluids partially wetting a solid surface [38,39]. The steady-state pinned profile with logarithmic tails given in Ref. [34] is taken as the initial condition. The equation of propagation can be solved exactly [30], yielding

$$\frac{\pi}{C}\frac{\delta v}{v_0} = \arctan\left(\frac{z+d}{v_0 t}\right) - \arctan\left(\frac{z-d}{v_0 t}\right). \tag{4}$$

From Eq. (4), we obtain the depinning velocity $v_{\mathrm{dep}} = Cv_0 \approx 3Cv_m$, which is in good agreement with the experimental data of Fig. 2(c) (solid line). Note that the existence of a characteristic depinning speed v_0 emerging from the kinetic law $G_c(v_m)$ was noticed by Kolvin *et al.* [40] in the context of microbranching induced crack pinning.

The speed profile can then be readily integrated to provide the general form of the front profile. Figure 4 shows a spatiotemporal map of $\delta f(z,t)$, where the entire relaxation to a straight configuration can be observed. To avoid cumbersome equations, we will just give analytical expressions of $\delta f(z,t)$ in some limits which are useful to interpret our experimental data [30]. For $z = d$, we obtain

$$\frac{\pi \delta f(d,t)}{Cd} = \frac{tv_0}{d}\left[\arctan\left(\frac{2d}{tv_0}\right) - 2\arctan\left(\frac{d}{tv_0}\right)\right] + \ln\left[\frac{4+(\frac{tv_0}{d})^2}{1+(\frac{tv_0}{d})^2}\right]. \tag{5}$$

Equation (5) is in good agreement with the experimental data of Fig. 3(b) (dashed line), using C_{NL} to normalize $\delta f(d,t)$. In the limit $|z| \gg d$, we obtain $\delta f(z,t) = Cd/\pi \ln(1 + [z/(tv_0)]^2)$, which generalizes the model of Marsh and Cazabat [41] for the depinning of a contact line, obtained in the long time and vanishing mean velocity limits [30]. Thus, we obtain

$$w(t) \simeq \sqrt{3} v_0 t = (\sqrt{3}/\gamma) v_m t. \tag{6}$$

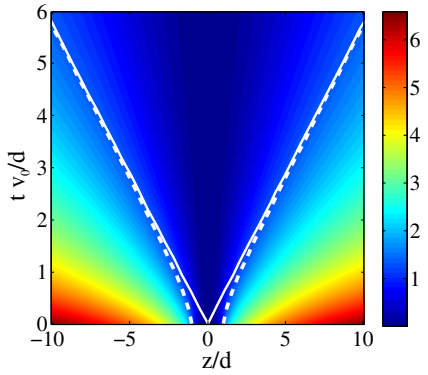

FIG. 4. Analytical spatiotemporal map of the front deformation δf during depinning. The contour line for $\delta f = \delta f_0$ obtained using the exact solution (dashed line) and the asymptotics solution for $|z| \gg d$ [Eq. (6), solid line] are shown.

As shown in Fig. 4, the linear spreading of the perturbation provides a good approximation even at relatively short time.

To summarize, our study of the depinning of a brittle crack from a single obstacle reveals a characteristic velocity v_0 that sets the relaxation time λ/v_0 of the front perturbations of wavelength λ. This characteristic speed that emerges from the crack growth law $G_c(v_m)$ allows us to derive an overdamped equation of motion $(v - v_m)/v_0 = [G - G_c(v_m)]/G_c(v_m)$ that was shown to capture quantitatively the crack front evolution during depinning as observed in our experiments. The offset between theory and experiments at longer time $t \gg d/v_0$ may be attributed to nonlinear geometrical effects [30]. Overall, a quasistatic theory captures well the depinning dynamics provided v_0 is much smaller than the Rayleigh wave speed $v_R \simeq 75$ m/s for PDMS.

Following are the implications of these findings. First, it sheds light on the nature of the dissipation accompanying avalanches in failure of heterogeneous solids. During an avalanche, the depinning region of the front reaches the speed v_0 that may be much larger than the average crack speed v_m. Owing to the increase of the fracture energy with crack speed and the continuity of the elastic energy at the onset of depinning, the dissipation rate during an avalanche is close to the toughness of the impurities, leading to an additional dissipation that reduces to $\simeq C^2 G_{c0} d^2$ per heterogeneity for the case of a periodic array of obstacles. For disordered distributions, in the strong pinning regime where the front motion consists of a succession of avalanches, we then expect the energy dissipated by the unit fractured surface to be significantly larger than the matrix toughness, and closer to the obstacle fracture energy, even for relatively low obstacle density. The proposed crack evolution equation that is amenable to the exploration of more complex toughness landscape embedding multiple obstacles predicts the total energy dissipated, including the contribution due to depinning instabilities, and so can serve

as a tool for the design of patterned interfaces with improved mechanical performance.

Secondly our findings allow us to address a long-standing question about the failure of disordered solids and its relationship with critical phenomena. For randomly distributed obstacles, cracks exhibit a jerky dynamics characterized by universal scaling laws that were shown to be reminiscent of the so-called depinning transition of an elastic interface driven in a random medium [22,25,42]. However, the control parameter that sets the distance of the system to the critical point was not identified yet, in particular, under displacement controlled conditions where the front velocity v_m is imposed. From the description of the crack dynamics during unstable events brought by this study, this can now be achieved through the comparison of the driving velocity v_m with the characteristic speed v_0 of the avalanches, leading to the control parameter $\delta = v_m/v_0$. As expected for dynamical phase transition, this parameter controls the crack front behavior, like the correlation time of the speed fluctuations that was recently shown to diverge as $1/\delta$ [28,29]. Interestingly, v_0 may not be independent of v_m. For many material systems like the one considered in this study, G_c increases as a power law of v_m so that $v_0 = v_m/\gamma$ [see Eq. (2)]. As a result, the control parameter may often take a fixed value $\delta = \gamma$, explaining why the crack response is independent of its average speed over several orders of magnitude [24,43]. Overall, the introduction of the parameter $\delta = v_m/v_0$ that controls the critical behavior of fracturing material opens a new perspective for the quantitative description of fracture in terms of depinning transition.

*julien.chopin@espci.fr
†laurent.ponson@upmc.fr

[1] B. Florijn, C. Coulais, and M. van Hecke, Phys. Rev. Lett. **113**, 175503 (2014).
[2] A. Leonard, L. Ponson, and C. Daraio, Extreme Mech. Lett. **1**, 23 (2014).
[3] M. K. Blees, A. W. Barnard, P. A. Rose, S. P. Roberts, K. L. McGill, P. Y. Huang, A. R. Ruyack, J. W. Kevek, B. Kobrin, D. A. Muller *et al.*, Nature (London) **524**, 204 (2015).
[4] K. Bertoldi, P. M. Reis, S. Willshaw, and T. Mullin, Adv. Mater. **22**, 361 (2010).
[5] J. L. Silverberg, A. A. Evans, L. McLeod, R. C. Hayward, T. Hull, C. D. Santangelo, and I. Cohen, Science **345**, 647 (2014).
[6] F. Lechenault, B. Thiria, and M. Adda-Bedia, Phys. Rev. Lett. **112**, 244301 (2014).
[7] H. Gao and J. R. Rice, J. Appl. Mech. **56**, 828 (1989).
[8] D. Dalmas, E. Barthel, and D. Vandembroucq, J. Mech. Phys. Solids **57**, 446 (2009).
[9] S. Patinet, L. Alzate, E. Barthel, D. Dalmas, D. Vandembroucq, and V. Lazarus, J. Mech. Phys. Solids **61**, 311 (2013).
[10] S. Xia, L. Ponson, G. Ravichandran, and K. Bhattacharya, J. Mech. Phys. Solids **83**, 88 (2015).
[11] M. Vasoya, A. B. Unni, J. B. Leblond, V. Lazarus, and L. Ponson, J. Mech. Phys. Solids **89**, 211 (2016).
[12] S. Roux, D. Vandembroucq, and F. Hild, Eur. J. Mech. A **22**, 743 (2003).
[13] M. Z. Hossain, C. J. Hsueh, B. Bourdin, and K. Bhattacharya, J. Mech. Phys. Solids **71**, 15 (2014).
[14] M. Vasoya, V. Lazarus, and L. Ponson, J. Mech. Phys. Solids **95**, 755 (2016).
[15] S. Xia, L. Ponson, G. Ravichandran, and K. Bhattacharya, Phys. Rev. Lett. **108**, 196101 (2012).
[16] A. Ghatak, Phys. Rev. E **89**, 032407 (2014).
[17] D. S. Kammer, D. P. Munos, and J. F. Molinari, J. Mech. Phys. Solids **88**, 23 (2016).
[18] F. Barthelat, J. Mech. Phys. Solids **73**, 22 (2014).
[19] D. Bonamy and E. Bouchaud, Phys. Rep. **498**, 1 (2011).
[20] M. J. Alava, P. K. Nukala, and S. Zapperi, Adv. Phys. **55**, 349 (2006).
[21] L. Ponson, Int. J. Fract. **201**, 11 (2016).
[22] J. Schmittbuhl, S. Roux, J. P. Vilotte, and K. J. Måløy, Phys. Rev. Lett. **74**, 1787 (1995).
[23] K. J. Måløy and J. Schmittbuhl, Phys. Rev. Lett. **87**, 105502 (2001).
[24] K. J. Måløy, S. Santucci, J. Schmittbuhl, and R. Toussaint, Phys. Rev. Lett. **96**, 045501 (2006).
[25] D. Bonamy, S. Santucci, and L. Ponson, Phys. Rev. Lett. **101**, 045501 (2008).
[26] J. Chopin, A. Boudaoud, and M. Adda-Bedia, J. Mech. Phys. Solids **74**, 38 (2015).
[27] L. Laurson, X. Illa, S. Santucci, K. T. Tallakstad, K. J. Måløy, and M. J. Alava, Nat. Commun. **4**, 2927 (2013).
[28] K. T. Tallakstad, R. Toussaint, S. Santucci, J. Schmittbuhl, and K. J. Måløy, Phys. Rev. E **83**, 046108 (2011).
[29] L. Ponson and N. Pindra, Phys. Rev. E **95**, 053004 (2017).
[30] See Supplemental Material at http://link.aps.org/supplemental/10.1103/PhysRevLett.121.235501 for the toughness characterization and the detailed calculation of the depinning dynamics.
[31] P.-G. de Gennes, C.R. Acad. Sci. Ser. Gen., Ser. 2 **307**, 1949 (1988).
[32] J. Chopin, R. Villey, D. Yarusso, E. Barthel, C. Creton, and M. Ciccotti, Macromolecules **51**, 8605 (2018).
[33] P.-P. Cortet, M.-J. Dalbe, C. Guerra, C. Cohen, M. Ciccotti, S. Santucci, and L. Vanel, Phys. Rev. E **87**, 022601 (2013).
[34] J. Chopin, A. Prevost, A. Boudaoud, and M. Adda-Bedia, Phys. Rev. Lett. **107**, 144301 (2011).
[35] M. Vasoya, J.-B. Leblond, and L. Ponson, Int. J. Solids Struct. **50**, 371 (2013).
[36] J. R. Rice, J. Appl. Mech. **52**, 571 (1985).
[37] N. Pindra, V. Lazarus, and J. B. Leblond, J. Mech. Phys. Solids **56**, 1269 (2008).
[38] P.-G. De Gennes, Rev. Mod. Phys. **57**, 827 (1985).
[39] E. Katzav, M. Adda-Bedia, M. BenAmar, and A. Boudaoud, Phys. Rev. E **76**, 051601 (2007).
[40] I. Kolvin, J. Fineberg, and M. Adda-Bedia, Phys. Rev. Lett. **119**, 215505 (2017).
[41] J. A. Marsh and A. M. Cazabat, Phys. Rev. Lett. **71**, 2433 (1993).
[42] L. Ponson, Phys. Rev. Lett. **103**, 055501 (2009).
[43] F. Plouraboué, K. W. Winkler, L. Petitjean, J. P. Hulin, and S. Roux, Phys. Rev. E **53**, 277 (1996).

Supplemental Material for "Depinning dynamics of crack fronts"

Julien Chopin[1,2,3], Aditya Bhaskar[2], Atharv Jog[2] and Laurent Ponson[2]
[1] *Gulliver UMR 7083, CNRS, ESPCI ParisTech, PSL Research University, F-75005 Paris, France*
[2] *Sorbonne Universités, UPMC Univ Paris 06, CNRS, UMR 7190, Institut Jean Le Rond d'Alembert, F-75005 Paris, France*
[3] Instituto de Física, Universidade Federal da Bahia, Salvador-BA 40170-115, Brazil
(Dated: November 12, 2018)

RATE DEPENDENCE OF THE FRACTURE ENERGY AND FRACTURE ENERGY CONTRAST

The rate dependence of the fracture energy G_{c0} of the neat (ink free) transparency/pdms interface is shown in Fig. 1(b). It has been obtained using the following procedure: the cantilever is pulled up at different rates in the range $\dot{\Delta} = 1 - 10\ \mu\text{m}.s^{-1}$. The force-displacement curve $F(\Delta)$ is then analyzed using the compliance method that provides the elastic energy release rate $G = F^2/(2b)d\lambda/dc$ as a function of time. Here, b is the specimen width along the crack front and $\lambda = \Delta/F$ the measured value of the compliance. The crack position and its evolution is determined using a camera, taking advantage of the transparency of the materials. The crack speed determined from the crack position is then represented in Fig. 1(b) as a function of the rate of dissipated energy that balances the elastic energy release rate. The data are modeled using the kinetic law $G_{c0} = (v_m/v_{c0})^{n_0}$, leading to $n_0 = 1/\gamma = 0.37 \pm 0.05$.

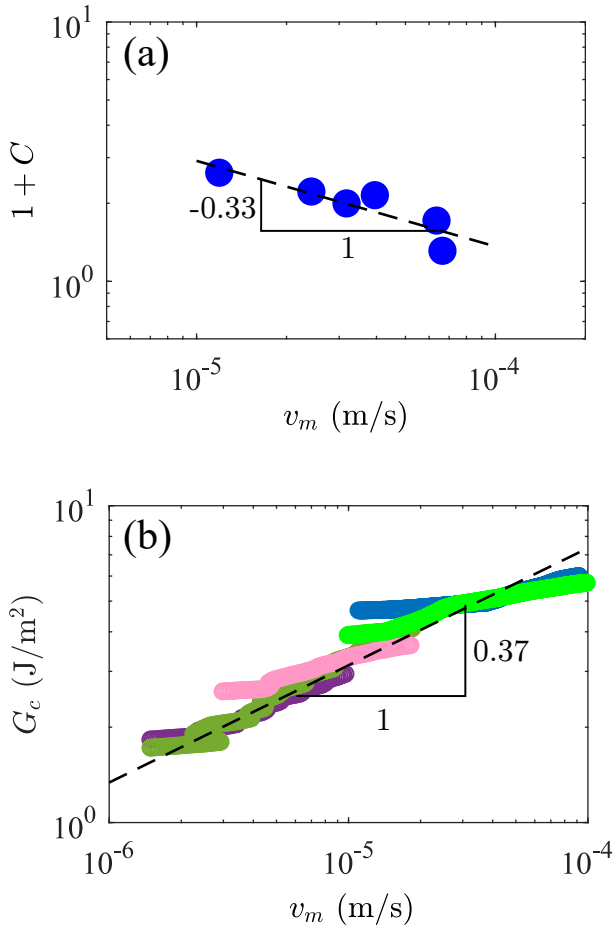

FIG. 1: (a) Evolution of the fracture energy contrast with the mean crack speed. A fit of the data provides $1 + C \sim v_{\text{m}}^{\Delta n}$ with $\Delta n = -0.33 \pm 0.07$. (b) Evolution of the fracture energy for a neat (ink-free) interface as a function of the crack mean speed obtained at different driving rates to cover a wider range. A fit of the data gives $G_{c0} = (v_{\text{m}}/v_{c0})^{n_0}$ with $v_{c0} = 0.45\ \mu\text{m.s}^{-1}$ and $\gamma = 0.37 \pm 0.05$.

The same procedure could not be performed with a homogeneous printed interface because the ink made the sample opaque preventing a visual detection of the crack front. However, the fracture energy of the inked interface can be derived from the fracture energy contrast. Assuming a similar kinetic law $G_{c1} = A_1(v_\mathrm{m}/v_{c1})^{n_1}$ for the inked interface, the contrast $C = (G_{c1} - G_{c0})/G_{c0}$ now reads

$$C + 1 = \frac{G_{c1}}{G_{c0}} = \left(\frac{v_0^{n_0}}{v_1^{n_1}}\right) v_m^{n_1 - n_0}. \tag{1}$$

Therefore, the contrast is found to be speed dependent with an exponent $\Delta n = n_1 - n_0$. Driving the crack front over a single defect at various speed, we can extract the contrast as explained in the main text. Figure 1(a) shows $C + 1$ as a function of the crack front mean speed v_m. From a fit of the data, we find $C + 1 \sim v_m^{\Delta n}$ with $\Delta n = -0.33 \pm 0.05$. Using the measured value $n_0 = 0.37$, we obtain $n_1 = \Delta n + n_0 = 0.04 \pm 0.05$. We thus conclude that the adhesion of the pdms on an inked interface has a negligible rate dependence compared to the neat interface.

THEORY

General solution of the crack evolution equation describing the depinning dynamics

Linear elastic fracture mechanics is used to model the depinning of an interfacial crack front from a single defect. The mechanical energy release rate, G, balances to the fracture energy, G_c, at any time along the evolving crack front, leading to

$$G_c(c(z,t), v(z,t)) \;=\; G(c(z,t)), \tag{2}$$

where $c(z,t)$ and $v(z,t) = \partial c(z,t)/\partial t$ are the absolute position and velocity fields of the crack front, respectively. In a homogeneous interface, $G_c(c(z,t), v(z,t)) \equiv G_c(v(z,t))$, since the fracture energy is identical along the crack front. Developing the fracture energy, $G_c(v(z,t))$, around the average speed, v_m, we get

$$G_c(v(z,t)) \;=\; G_c(v_m) + \left.\frac{\partial G_c}{\partial v}\right|_{v=v_m} \times (v(z,t) - v_m). \tag{3}$$

Introducing the characteristic velocity v_0 defined by $v_0 = G_c(v_m)/\left.\frac{\partial G_c}{\partial v}\right|_{v=v_m}$ and defining $\delta c(z,t) = c(z,t) - v_m t$, Eq. (3) is rewritten as

$$G_c \;=\; G_c(v_m) + \frac{G_c(v_m)}{v_0}\frac{\partial \delta c(z,t)}{\partial t}. \tag{4}$$

Additionally by expanding the energy release rate, G, using a first-order perturbation valid for an interfacial crack between an incompressible elastic material and a rigid substrate, we have,

$$G \;=\; G_{ext} + \frac{G_{ext}}{\pi} PV \int_{-\infty}^{+\infty} \frac{\delta c(z',t) - \delta c(z,t)}{(z'-z)^2} dz'. \tag{5}$$

Using the Griffith criterion, $G_c(v_m) = G_{ext}$, and Eqs. (2), (4) and (5), we get the following governing integro-differential equation for the evolving crack front

$$\frac{1}{v_0}\frac{\partial \delta c(z,t)}{\partial t} \;=\; \frac{1}{\pi} PV \int_{-\infty}^{+\infty} \frac{\delta c(z',t) - \delta c(z,t)}{(z'-z)^2} dz'. \tag{6}$$

Using the technique of variable separation, $\delta c(z,t) = \alpha(t)\beta(z)$, we rewrite Eq. (6) as

$$\frac{1}{v_0}\frac{1}{\alpha(t)}\frac{d\alpha(t)}{dt} \;=\; \frac{1}{\pi}\frac{1}{\beta(z)} PV \int_{-\infty}^{+\infty} \frac{\beta(z') - \beta(z)}{(z'-z)^2} dz' = k \in \mathbb{C}, \tag{7}$$

$$\Rightarrow \alpha(t) \;=\; e^{k v_0 t}. \tag{8}$$

The multiplicative constant in the solution for $\alpha(t)$ has been dropped as it can be absorbed in the solution for $\beta(z)$. Owing to the relaxation process, we require the front deformation $\delta f(z,t) = \delta c(z,t) - \delta c(0,t)$ defined from the point

of the crack line located in $z = 0$ to vanish at very long time. This restricts the range of k to negative real numbers. Further, assuming the solution $\beta(z)$ to be equal to its Taylor expansion and bounded, we have, by integration-by-parts applied to the finite-part integral,

$$\frac{1}{\pi} PV \int_{-\infty}^{+\infty} \frac{\beta'(z')}{z'-z} dz' \;=\; k\beta(z). \tag{9}$$

We perform a Hilbert transform on Eq. (9) and then use the anti-involution property of the Hilbert transform. We also differentiate Eq. (9) and then use the commutative property of the Hilbert operator and the derivative operator, resulting in two equations,

$$\beta'(z) \;=\; k.\mathcal{H}\{\beta(z)\} = \frac{-\mathcal{H}\{\beta''(z)\}}{k}.$$

Using the Hilbert transform on the equation and the anti-involution property again we get

$$\begin{aligned} \beta''(z) &= -k^2\beta(z), \\ \Rightarrow \beta(z) &= K_1 e^{ikz} + K_2 e^{-ikz}, \end{aligned} \tag{10}$$

$$\Rightarrow \delta c_k(z,t) \;=\; K_1 e^{ikz+kv_0t} + K_2 e^{-ikz+kv_0t}, \;\; k \in \mathbb{R}^-. \tag{11}$$

Since any linear combination of the solutions of Eq. (6) is also a solution to the equation, we obtain the most general solution by taking a linear combination of solutions for all allowed values of k, which passes to an integral in the limit,

$$\begin{aligned} \delta c(z,t) &= \int_{-\infty}^{0} \psi(k)(K_1 e^{ikz+kv_0t} + K_2 e^{-ikz+kv_0t})dk, \\ \Rightarrow \delta c(z,t) &= \int_{-\infty}^{+\infty} \phi(k) e^{ikz-|k|v_0t} dk. \end{aligned} \tag{12}$$

$\phi(k)$ can be specified using the initial crack shape, $\delta c(z,0) = c(z,0)$. For a square-integrable function, $c(z,0)$, and due to Plancherel's theorem, one obtains

$$\phi(k) \;=\; \frac{1}{2\pi} \int_{-\infty}^{+\infty} c(z,0) e^{-ikz} dz. \tag{13}$$

Since $\phi(k)$ can be found for any given $c(z,0)$, it implies that this linear combination of the variable-separable solutions is in fact the most general solution.

Kinematic equations of a crack depinning from a single defect

We apply the result obtained in the previous section to the special case of a crack depinning from a single defect. The initial crack front is described by the function [1]

$$\phi(k) = -C \frac{\sin(kd)}{\pi k|k|} \tag{14}$$

where d is the half-width of the obstacle with $z = \pm d$ being its sides. C is the contrast parameter defined by the relation $C = (G_{c1} - G_{c0})/G_{c0}$, where G_{c1} is the fracture toughness of the obstacle and G_{c0} is the fracture energy of the matrix. This initial crack profile, $\phi(k)$, is obtained by considering a single elongated obstacle and calculating the Fourier transform of the perturbed crack front up to the first order. The expression of the perturbed profile in real space reads [2]:

$$\delta c(z,0) = c(z,0) = \frac{C\,d}{\pi} \left[\left(1 + \frac{z}{d}\right) \ln\left|1 + \frac{z}{d}\right| + \left(1 - \frac{z}{d}\right) \ln\left|1 - \frac{z}{d}\right| \right]. \tag{15}$$

In the limit where $|z/d| \gg 1$, we obtain the logarithmic tails of the perturbation $\delta c(z,0) \approx 2Cd/\pi \ln|z/d|$. Second order corrections can be found in [1]. The steady state profile is used as an initial condition for analyzing the dynamical propagation of the crack. Using Eq. (12) and performing symmetrical integration, we obtain

$$\delta v(z,t) \;=\; \frac{\partial \delta c(z,t)}{\partial t} = \frac{Cv_0}{\pi} \int_0^{\infty} \frac{2\sin(kd)\cos(kz)}{k} e^{-kv_0t} dk. \tag{16}$$

To compute the integral, we rewrite $\delta v(z,t)$ as

$$\delta v(z,t) \;=\; \lim_{t\to\infty}\delta v(z,t) - \int_t^{\infty}\frac{\partial \delta v(z,t)}{\partial t}dt. \tag{17}$$

Since the front is driven at a velocity $v_{\rm m}$, after a long period of time, we apply the boundary condition $\lim_{t\to\infty}\delta v(z,t)=0$ and calculate the velocity field, $\delta v(z,t)$, using the Leibniz integral rule

$$\begin{aligned}\delta v(z,t) \;&=\; -\frac{Cv_0}{\pi}\int_{t=t}^{t\to\infty}\frac{\partial}{\partial t}\left(\int_{k=0}^{k\to\infty}\frac{2\sin(kd)\cos(kz)}{k}e^{-kv_0t}dk\right)dt,\\ \Rightarrow \delta v(z,t) \;&=\; \frac{Cv_0}{\pi}\left(\arctan\left(\frac{v_0t}{d+z}\right)\Big|_{t=t}^{t\to\infty}+\arctan\left(\frac{v_0t}{d-z}\right)\Big|_{t=t}^{t\to\infty}\right).\end{aligned} \tag{18}$$

Upon using the limiting conditions, we get the following two cases

$$\delta v(z,t) \;=\; \frac{Cv_0}{\pi}\left(\arctan\left(\frac{v_0t}{z-d}\right)-\arctan\left(\frac{v_0t}{z+d}\right)\right), \qquad |z|>d \tag{19}$$

$$\delta v(z,t) \;=\; \frac{Cv_0}{\pi}\left[\pi-\left(\arctan\left(\frac{v_0t}{d+z}\right)+\arctan\left(\frac{v_0t}{d-z}\right)\right)\right], \qquad |z|<d. \tag{20}$$

We note in particular that

$$v_0=\delta v(|z|<d,0^+)/C. \tag{21}$$

Thus we get a new interpretation for the parameter, v_0, as being proportional to the speed jump inside the defect, $\delta v(|z|<d,0^+)$ at the onset of depinning. This jump in the velocity is a consequence of the continuity of the crack profile with respect to time and the sudden turn off of the toughness contrast. Before depinning, the elastic restoring force due to the crack fluctuations are balanced by the pinning force. At the depinning transition, the toughness contrast is set to zero, thus, the same elastic restoring force are now balanced by viscous dissipation. This results in a speed jump in the region $|z|<d$ whose amplitude is adjusted so that viscous friction is equal to the pinning force. This condition of continuity yields Eq. (21) We further note that in the long-time limit, $v_0t/d\gg 1$, Eqs. (19) and (20) reduce to an expression independent of z to give

$$v(z,t)|_{v_0t/d\gg 1} \;=\; v_m+\frac{2dC}{\pi t}. \tag{22}$$

The crack displacement field can be evaluated by direct integration of Eqs. (19) and (20) with respect to time. To circumvent mathematical difficulties related to integration, we evaluate the displacement field measured from a frame attached to the moving origin, $\delta f(z,t)=c(z,t)-c(0,t)$, by integrating, $\delta\dot f(z,t)=v(z,t)-v(0,t)$. The boundary condition used is $\lim_{t\to\infty}\delta f(z,t)=0$. Again considering two separate cases of $|z|>d$ and $|z|<d$, we obtain

$$\int_t^{\infty}\delta\dot f(|z|>d,t)dt = 0-\delta f(|z|>d,t) = \int_t^{\infty}\frac{Cv_0}{\pi}\left(\arctan\left(\frac{v_0t}{z-d}\right)-\arctan\left(\frac{v_0t}{z+d}\right)-\pi+2\arctan\left(\frac{v_0t}{d}\right)\right)dt$$

$$\begin{aligned}\Rightarrow \delta f(|z|>d,t) \;=\; \frac{Cv_0}{\pi}\Bigg[&t\left(-\pi+2\arctan\left(\frac{v_0t}{d}\right)+\arctan\left(\frac{v_0t}{z-d}\right)-\arctan\left(\frac{v_0t}{z+d}\right)\right)-\left(\frac{d}{v_0}\right)\ln\left(d^2+(v_0t)^2\right)\\ &+\left(\frac{z+d}{2v_0}\right)\ln\left((z+d)^2+(v_0t)^2\right)-\left(\frac{z-d}{2v_0}\right)\ln\left((z-d)^2+(v_0t)^2\right)\Bigg]\end{aligned} \tag{23}$$

$$\int_t^{\infty}\delta\dot f(|z|<d,t)dt \;=\; 0-\delta f(|z|<d,t) = \int_t^{\infty}\frac{Cv_0}{\pi}\left(2\arctan\left(\frac{v_0t}{d}\right)-\arctan\left(\frac{v_0t}{d+z}\right)-\arctan\left(\frac{v_0t}{d-z}\right)\right)dt$$

$$\begin{aligned}\Rightarrow \delta f(|z|<d,t) \;=\; \frac{Cv_0}{\pi}\Bigg[&t\left(2\arctan\left(\frac{v_0t}{d}\right)-\arctan\left(\frac{v_0t}{d+z}\right)-\arctan\left(\frac{v_0t}{d-z}\right)\right)-\left(\frac{d}{v_0}\right)\ln\left(d^2+(v_0t)^2\right)\\ &+\left(\frac{d+z}{2v_0}\right)\ln\left((d+z)^2+(v_0t)^2\right)+\left(\frac{d-z}{2v_0}\right)\ln\left((d-z)^2+(v_0t)^2\right)\Bigg].\end{aligned} \tag{24}$$

Thus, in this work we have found the temporal evolution of the steady state shape when the front leaves the pinning sites. It can be noted that at the initial time i.e. $t \to 0$, we recover the steady state profile obtained by Chopin et al. [2] (see Eq. (15)).

The displacement function of the origin is also calculated using Eq. (20),

$$\int_0^t v(0,t)dt = \int_0^t \left(v_m + \frac{Cv_0}{\pi} \left[\pi - 2 + \arctan\left(\frac{v_0 t}{d}\right) \right] \right) dt \tag{25}$$

$$c(0,t) = c(0,0) + v_m t + Cv_0 t - \frac{2Cv_0}{\pi} \left[t \times \arctan\left(\frac{v_0 t}{d}\right) - \frac{d}{2v_0} \ln\left(1 + \left(\frac{v_0 t}{d}\right)^2\right) \right]. \tag{26}$$

Front evolution in the case of a thin defect and slow mean speed: $d/|z| \ll 1$**,** $v_0 t/d \gg 1$ **and** $v_m/Cv_0 \ll 1$

Using the Taylor approximation, for $\Delta \approx 0$, we can write,

$$f(x+\Delta) - f(x-\Delta) - 2f(\Delta) = 2\Delta(f'(x) - f'(0)) - 2f(0). \tag{27}$$

Substituting Eq. (27) into the trigonometric and logarithmic terms in Eq. (23) we get,

$$\begin{aligned}
\delta f(z,t)|_{d/|z|\ll 1} &= 2d\left(\frac{d}{dz}\left(C\frac{v_0 t}{\pi}\left(\arctan\left(\frac{z}{v_0 t}\right)\right)\right) - \frac{d}{dz}\left(C\frac{v_0 t}{\pi}\left(\arctan\left(\frac{z}{v_0 t}\right)\right)\right)_{z=0}\right) \\
&\quad + 2d\left(\frac{d}{dz}\left(C\frac{v_0}{\pi}\left(\frac{z}{2v_0}\ln(z^2+(v_0 t)^2)\right)\right) - \frac{d}{dz}\left(C\frac{v_0}{\pi}\left(\frac{z}{2v_0}\ln(z^2+(v_0 t)^2)\right)\right)_{z=0}\right), \\
&= C\frac{-2dz^2}{\pi[z^2+(v_0 t)^2]} + C\frac{2dv_0}{\pi}\left[\frac{2z^2}{2v_0[z^2+(v_0 t)^2]} + \frac{\ln(z^2+(v_0 t)^2)}{2v_0} - \frac{\ln((v_0 t)^2)}{2v_0}\right],
\end{aligned}$$

$$\Rightarrow \delta f(z,t)|_{d/|z|\ll 1} = \frac{Cd}{\pi}\ln\left(1+\left(\frac{z}{v_0 t}\right)^2\right). \tag{28}$$

We now express Eq. 28 in the moving frame of reference. Using Eqs. (26) and 28, we have,

$$\begin{aligned}
c(z,t)|_{d/|z|\ll 1} &= \frac{Cd}{\pi}\ln\left(1+\left(\frac{z}{v_0 t}\right)^2\right) + c(0,0) + v_m t + Cv_0 t \\
&\quad - \frac{2Cv_0}{\pi}\left[t \times \arctan\left(\frac{v_0 t}{d}\right) - \frac{d}{2v_0}\ln\left(1+\left(\frac{v_0 t}{d}\right)^2\right)\right].
\end{aligned} \tag{29}$$

Eq. 30 can be further simplified considering the long time limit, $v_0 t/d \gg 1$, slow mean speed, $v_m/Cv_0 \ll 1$, and set the arbitrary reference $c(0,0) = 0$. From Eq. (29) we get,

$$c(z,t)|_{d/|z|\ll 1, v_0 t/d \gg 1, v_m/Cv_0 \ll 1} = \frac{Cd}{\pi}\ln\left(\frac{z^2+(v_0 t)^2}{d^2}\right) \tag{30}$$

Thus we have retrieved the depinning dynamics of a contact line, derived by Marsh & Cazabat [3] for thin defect ($|z|/d \gg 1$), in the long time limit ($v_0 t/d \gg 1$) and low mean velocity ($v_m/Cv_0 \ll 1$). Incidentally, our derivation illuminates the various approximations implicitly used in the model developed by Marsh & Cazabat.

Finally, we would like to discuss the linear approximation made in our model. The distribution of elastic energy release rate along the front is given by a first-order development of $G[f(z)]$, leading to a linear variation of δG with the front perturbations δc (see Eq. (5)). This amounts to assume that the crack front is weakly perturbed, and more specifically, that its slope is small, $f(z) \ll 1$. This is somehow contradictory with the initial condition Eq. (15) of the crack configuration as the slope $\delta c'(z)$ actually diverge in $z = \pm d$. This may explain why the predicted values of w lie below the experimental data in Fig. 3b, suggesting that the theory underestimates the speed at which the relaxation process and the spreading of the front perturbation take place. Indeed, as shown in Ref. [1], geometrical non-linear

effects result in a stronger elasticity (i.e. an increased stiffness) of the crack front, and so in a larger depinning speed. Even though this effect might explain a slightly faster depinning process in the experiments as compared to the predictions of our linear theory, the region where the crack front slope is large is actually very small, so that the linear theory proposed in this study captures overall well the relaxation dynamics of a crack from a tough obstacle.

[1] M. Vasoya, J.-B. Leblond, and L. Ponson, Int. J. Solids Struct. **50**, 371 (2013).
[2] J. Chopin, A. Prevost, A. Boudaoud, and M. Adda-Bedia, Phys. Rev. Lett. **107**, 144301 (2011).
[3] J. Marsh and A. Cazabat, Physical review letters **71**, 2433 (1993).